Contrib Mineral Petrol (2006) 152:349–364
DOI 10.1007/s00410-006-0110-7

ORIGINAL PAPER

Episodic mineralization of hydrothermal illite in the Soultz-sous-Forêts granite (Upper Rhine Graben, France)

Anja M. Schleicher · Laurence N. Warr · Bernd Kober · Emmanuel Laverret · Norbert Clauer

Received: 5 July 2005 / Accepted: 26 May 2006 / Published online: 27 July 2006

Abstract Episodic and localized illite mineralization is documented in the hydrothermally altered Soultz-sous-Forêts granite (Upper Rhine Graben, France). Separated grain-size fractions of altered granite and argillite vein samples contain mixtures of $2M_1$ and 1M trans-vacant illite varieties. The platy pseudohexagonal $2M_1$ illite phases dominate the vein fillings, whereas the 1M illite occurs largely as a fibrous pore-filling variety, which is particularly abundant in the granite matrix. Multiple phases of fluid injections into the granite body have resulted in different illite assemblages, each sample containing a mixture of polytype generations formed during different crystal growth events. On the basis of mineralogical and K–Ar isotopic constraints, the ages of these vein-mineralizing events are determined by plotting the K–Ar values of the various grain-size fractions against polytype abundance and the fitted volume-weighted crystallite thickness distributions. The results suggest a Permian age for the formation of the studied argillite veins, characterized by successive injections of hydrothermal fluids. Secondary episodes of illite crystallization occurred during Jurassic and Cretaceous (or even younger times) in both the veins and the granite matrix. There are indications that the polytype structure and composition of illite were strongly influenced by variations in fluid chemistry and the degree of fluid–rock interaction as the granite was progressively sealed during post-Variscan, episodic hydrothermal activity.

Keywords Illite · Hydrothermal fluids · Granite · Rhine Graben · Soultz-sous-Forêts · K–Ar age values · Permian veins

Communicated by T.L. Grove

A. M. Schleicher (✉)
Geologisch-Paläontologisches Institut,
Ruprecht-Karls-Universität INF 234,
69120 Heidelberg, Germany
e-mail: anja.schleicher@urz.uni-heidelberg.de

L. N. Warr · N. Clauer
Centre de Géochimie de la Surface (CNRS-ULP),
1 rue Blessig, 67084 Strasbourg, France

B. Kober · E. Laverret
Institut für Umweltgeochemie, Ruprecht-Karls-Universität
INF 234, 69120 Heidelberg, Germany

Introduction

Illite is recognized as an important mineral phase for reconstructing the geological history of fluid–rock interactions in most diagenetic, hydrothermal, and very-low-grade metamorphic settings (e.g. Clauer and Chaudhuri 1995; Inoue et al. 2004; Merriman and Frey 1999). The usefulness of this mineral relates to its widespread occurrence in the broad range of subsurface low-temperature geological environments ($<300°C$), its diverse crystal–chemical structure, and its relatively high K-content that allows it to be dated using well-established K–Ar or $^{40}Ar/^{39}Ar$ isotopic techniques (Bailey et al. 1962; Hunziker et al. 1986; Clauer et al. 1995a, b, 2003; Imaoka et al. 2001; Altaner et al. 2003). Although there are known analytical complications associated with the reliable study of illite due to its small particle size and common mixed-layered structure, this mineral phase continues to provide a powerful tool for elucidating the timing and mechanisms of low-temperature crystallizations in rocks

(Bailey et al. 1962; Clauer and Kröner 1979; Clauer et al. 1995a, b).

In addition to direct observations of intact samples by electron microscopy, a main technique applied in studying complex illite mixtures is to separate and analyze the range of grain sizes present within rocks. This approach is common when investigating clastic sedimentary successions (Hower et al. 1963; Clauer et al. 1995a, b; Rousset and Clauer 2003; Liewig and Clauer 2000; Reuter 1985), fault gouges (van der Pluijm 1999; van der Pluijm et al. 2001), and altered volcanic and igneous rocks (Glasmacher et al. 2001; Honty et al. 2004). In such studies, the material is separated into several grain sizes, and the mineralogical and isotopic signatures interpreted from the way the crystal–chemical characteristics vary in the different fractions. In most natural illite assemblages, the finest size fraction (e.g. <0.2 μm) is typically dominated by younger illite and the coarse fraction by older K-mica (or K-feldspar) phases. In the case of isotopic dating, when a mixture of two such components are present in all grain-size fractions, the youngest and oldest end-member values are generally considered to approach the true ages of the illite components present (Hunziker et al. 1986).

The key features in resolving the history of illite crystallization from complex argillite assemblages are the direct observations of crystal shape and size (Srodon et al. 2002), the analysis of illite compositions (Yates and Rosenberg 1998; Srodon 1984), the identification of polytype structures (Hunziker et al. 1986; Grathoff et al. 2001; Grathoff and Moore 2002), and more recently, the measurement of crystallite thickness distributions (CTDs; Eberl et al. 1987; Kim and Peacor 2002). Until now, the most widely adopted method to identify and separate different generations of illite is to determine and quantify illite polytypes (1M and 2M varieties) in separated grain-size fractions by powder X-ray diffraction methods (Drits et al. 1997; Grathoff and Moore 2002). Such constraints are plotted against the K–Ar values to extrapolate modeled illite ages from the graphical intercepts that represent pure end-member phases (Hunziker et al. 1986; Clauer and Chaudhuri 1995; Ylagan et al. 2002; Laverret 2002).

In this study, we investigate the nature of illite in the hydrothermally altered granite from the Soultz-sous-Forêts borehole, located in the Upper Rhine rift valley, France. The mineral assemblages of this granite body are particularly suitable for unraveling the crystallization history because: (1) the alteration products of the granite result from direct precipitation during hydrothermal fluid migration, with no magmatic micas present in the fine-grain sizes, (2) the samples are generally K-rich (3–11 wt%) enabling accurate determination of the K–Ar systematics, (3) the separated fractions consist mostly of discrete illite with many of the finer fractions approaching monomineralic composition, and (4) a variety of characteristic crystal shapes and polytypes occur in varying concentrations within each sample studied. On the basis of X-ray diffraction (XRD), scanning electron microscopy (SEM), transmission electron microscopy (TEM), and K–Ar study of this relatively pure material, it is shown that how combining these methods allows us to establish the complex timing and mechanisms of episodic illite crystallization in this well-documented granite intrusion.

Although a significant number of studies have characterized the nature of hydrothermal alteration in the Soultz-sous-Forêts granite, little attention has been given to the characterization and isotopic dating of the illite formed during this alteration. Despite the general lack of age constraints, many of the fractures and associated argillitic mineralization are often assumed to be relatively young and are attributed to Oligocene (or younger) rifting episodes in the Rhine Graben (Dubois et al. 1996; Genter and Traineau 1996; Elsass et al. 1995).

The geological setting

The Soultz-sous-Forêts granite is located in the northwestern region of Alsace (France) and forms part of the crystalline basement buried within the western part of the Tertiary Upper Rhine rift system (Fig. 1). Owing to the high geothermal gradient (up to 100°C/km), it has been selected as a test site for the recovery of thermal energy, and is currently being investigated within the framework of the European Hot Dry Rock Project (Genter et al. 2000). In the 2,230-m deep EPS-1 borehole located in an N–S striking horst structure, the contact between sedimentary cover rocks and the granite was encountered at a depth of 1,420 m.

The investigated granite belongs to a series of late to post-tectonic Variscan granitoids that occur in the Vosges mountains, and have been dated by various isotopic methods (Bonhomme et al. 1975; Montigny and Faure 1969). The Soultz granite is a porphyritic variety with K-feldspar megacrysts, quartz, plagioclase, biotite, hornblende and accessory apatite, titanite, and magnetite (Genter and Traineau 1991). Its age of crystallization has been dated by Alexandrov et al. (2001) to be 331 ± 9 Ma based on the U–Pb study of zircons. It is well established that the entire pluton was affected by an early hydrothermal pervasive (propylitic) alteration, followed by more localized fluid

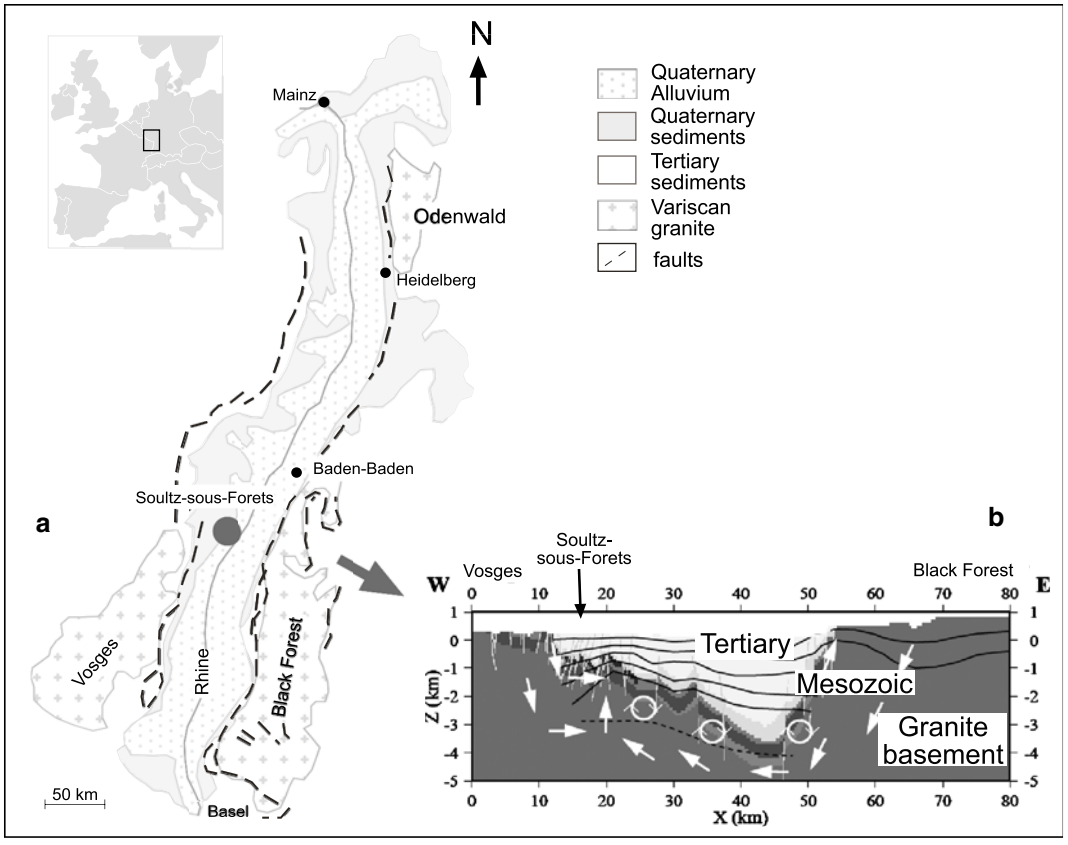

Fig. 1 **a** Location map showing the Upper Rhine Graben rift and the position of the Soultz-sous-Forêts hydrothermal borehole (*EPS-1*). **b** The geological cross-section (modified after Pribnow and Clauser 2000) presents an E–W profile across the southern part of the rift. *Subvertical structures* are fault zones, the *arrows* indicate the direction of fluid flow

percolations leading to the mineralization of siliceous and argillitic vein assemblages, as well as younger, fracture-related precipitations (Sausse et al. 1998). Secondary vein minerals are heterogeneous and contain predominantly quartz, barite, pure white mica (illite), carbonates, and iron oxides, with some localized mixed-layered illite–smectite and chlorite–smectite (tosudite) minerals (Genter and Traineau 1991; Ledesert et al. 1999). On the basis of fluid inclusion studies (Dubois et al. 1996), the earliest stage of pervasive alteration is characterized by fluids of moderate salinity (2–7 wt% eq. NaCl) trapped under temperatures of 180–340°C. These fluids were suggested to be of late Variscan age. A subsequent generation of lower temperature brines (ca. 130–160°C) with a large salinity range were also recognized in quartz-barite veins, and attributed to younger, post-Oligocene fluid-flow events (Dubois et al. 1996).

Sampling and analytical procedure

The studied material comes from the EPS-1 borehole, which has been continuously cored to a depth of 2,230 m. Two representative samples of whole-rock granite and three argillite veins were selected from different sections of the borehole profile (Fig. 2). The shallowest sample studied (vein-1) is located just beneath the unconformity at a depth of 1,431 m and consists of a cataclased porphyric granite containing an argillite (illite-rich) vein. About 140 m deeper into the core section (1,570 m), pervasively altered granite that lacks visible fracturing (granite-1) was taken. The remaining three samples were all selected from the lower section of the core between 2,160 and 2,176 m, and lie within a fracture zone characterized by active fluid flow (Genter and Traineau 1996). These samples comprise one hydrothermally altered host-rock granite (granite-2) and two argillite veins (2 and 3) of precipitated illite and quartz.

For XRD and K–Ar analyses, parts of these rock samples were initially hand-crushed into small millimeter-sized fragments and white-to-pale-green argillaceous-rich rock portions selected by hand. A total of eight grain-size fractions (>63, 10–63, 4–10, 2–4, 1–2, 0.4–1, 0.2–0.4, and <0.2 μm) were separated using a combination of wet-disaggregation, sedimentation, and

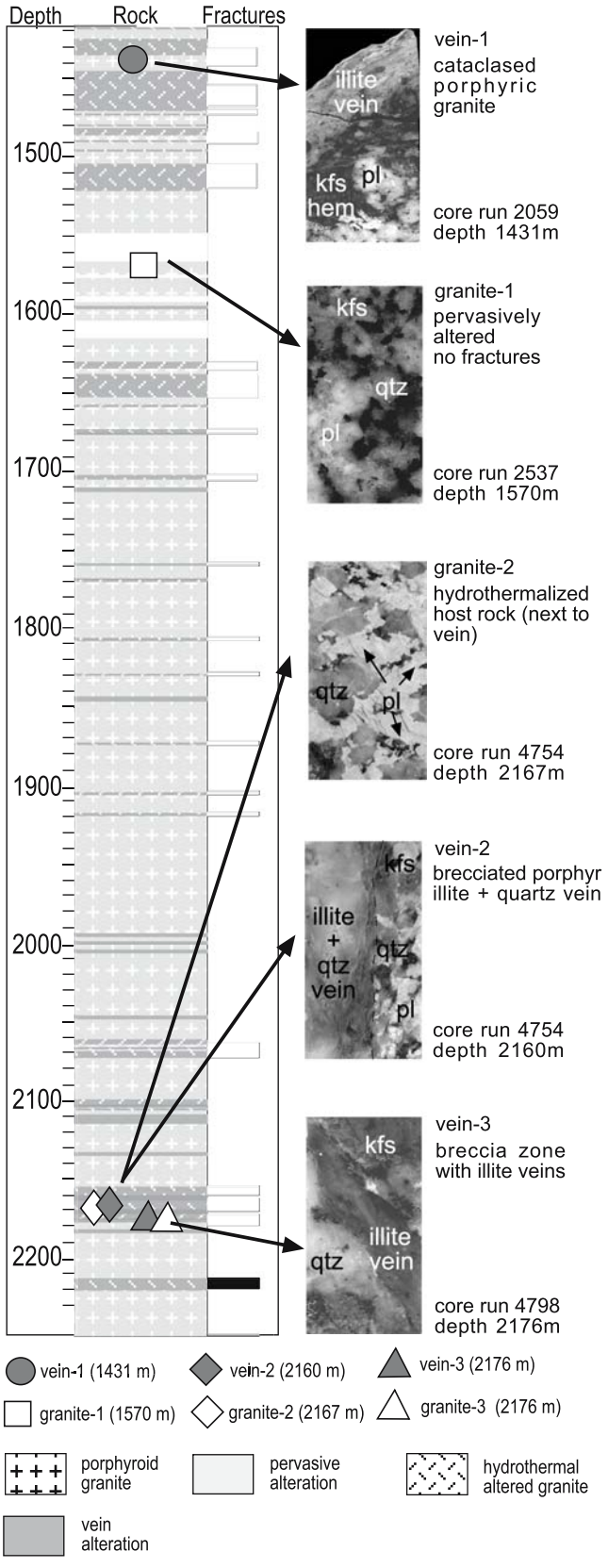

◀ **Fig. 2** Lithologic section of the *EPS-1* drill core at the 1,414–2,230-m depth interval (modified after Genter and Traineau 1996). The investigated five samples were selected from different depths, consisting of two whole rock granites and three argillaceous veins. The sample numbers are according to the nomenclature of the core index

centrifugation techniques described in detail by Schleicher (2005). The wt% of each grain-size range was also determined as a proportion of the whole-rock fraction (Table 1).

XRD analyses of random powder and texture preparations followed the analytical methods described by Moore and Reynolds (1997). For calculation of the CTD, thin films were prepared following the method of Eberl et al. (1998a, b). Mixtures of 2.5 mg of Na-saturated clay and 2.5 ml of distilled water were dispersed ultrasonically and pipetted onto a silicon wafer to reduce background effects. Initial measurements of representative fine fractions (including the finest grain sizes) were made following air-dried, ethylene glycol, or polyvinylpyrrolidone (PVP) treatments. The CTDs show no significant differences in the best mean thickness (T) or shape parameters (α and β^2) measured (Fig. 3). This indicates that any variation in XRD peak shape reflects crystallite thickness and not the presence of mixed-layered smectite in these samples. To minimize sample treatment and potential preparation damage (Warr and Peacor 2002), air-dried and non-PVP-treated samples were used for the routine determination of CTD. Repeat measurements of size fractions showed good reproducibility of the results, even for the coarser samples (<10 μm) where the calculated CTDs are expected to be most sensitive to textural variations. Polytype identification was based on the diffraction criteria of Drits et al. (1993) and a quantification of polytype abundance was made using the relative intensities at 3.07 and 3.66 Å for $1M_{tv}$ and 3.88, 3.72, 3.49, 3.2, 2.98, and 2.86 Å for $2M_1$ polytypes, respectively (Moore and Reynolds 1997; Laverret 2002). Owing to the problem of overlapping feldspar reflections in granite samples, quantification was only applied to the illite XRD patterns of the vein samples.

For SEM investigation, small rock fragments were used for secondary electron imaging, and polished thin sections for backscattered electron study. Qualitative analyses of mineral composition were obtained by energy-dispersive spectroscopy (EDS). Key samples were then selected and investigated using high-resolution TEM and analytical electron microscopy (AEM) techniques following the analytical procedures outlined

Table 1 List of the data used in this study determined by X-ray diffraction analyses for the five studied vein and granite samples

Sample (depth/m)	Whole rock minerals	Fine fraction minerals	Grain size (μm)	Weight (%)	Intensity 001 peak (cps)	FWHM 001 peak (°2θ)	Area-weighted			Volume weighted % mean CT		Polytype	
							Best mean	α	β^2	pC	wC	%1Mt (3.07 Å)	%$2M_1$ (3.2 Å)
Vein-1 (1,431 m)	K-feldspar, plagioclase, quartz, hematite, dolomite	Illite, quartz	<2	–	9542	0.36	–	–	–	–	–	–	–
			<0.2	–	2461	0.28	–	–	–	–	–	–	–
Granite-1 (1,570 m)	K-feldspar, plagioclase, quartz, biotite, dolomite	Illite, quartz, plagioclase	<63	92.2	22355	0.17	–	–	–	–	–	–	–
			10–63	4.86	35751	0.21	34	3.22	0.23	–	–	–	
			4–10	1.02	13665	0.22	24	2.84	0.45	–	–	–	
			2–4	0.71	9531	0.29	18	2.50	0.64	–	–	–	–
			1–2	0.70	4485	0.50	10	2.17	0.55	–	–	–	–
			0.4–1	0.40	3754	0.63	7	2.05	0.59	–	–	–	–
			0.2–0.4	0.19	2639	0.76	5	1.73	0.39	–	–	–	–
			<0.2	0.04	2190	0.84	6	1.71	0.42	–	–	–	–
Granite-2 (2,167 m)	K-feldspar, plagioclase, quartz, illite veins	Illite, quartz	<63	78.90	–	–	–	–	–	–	–	–	–
			10–63	9.66	3118	0.40	8	2.07	0.51	–	–	–	–
			4–10	2.34	6754	0.40	9	2.17	0.43	–	–	–	–
			2–4	2.54	13696	0.38	10	2.23	0.36	–	–	–	–
			1–2	1.67	17905	0.40	12	2.32	0.31	–	–	–	–
			0.4–1	0.66	40203	0.44	14	2.47	0.28	–	–	–	–
			0.2–0.4	2.19	38739	0.62	11	2.27	0.22	–	–	–	–
			<0.2	0.82	–	–	8	2.05	0.18	–	–	–	–
Vein-2 (2,160 m)	Illite, feldspar, quartz, dolomite	Illite, quartz, dolomite	<63	79.20	–	–	–	–	–	–	–	–	–
			10–63	8.31	4759	0.35	8	1.98	0.62			–	–
			4–10	2.53	7719	0.46	11	2.37	0.42	35	–	19	81
			2–4	2.23	27298	0.33	14	2.51	0.36	36	65	27	73
			1–2	1.56	36342	0.32	17	2.65	0.30	38	64	43	57
			0.4–1	3.66	48949	0.39	17	2.71	0.28	43	62	66	34
			0.2–0.4	0.89	46313	0.45	16	2.62	0.26	69	57	76	24
			<0.2	1.31	42924	0.46	13	2.52	0.27	100	31	87	13
Vein-3 (2,176 m)	Illite, quartz, dolomite, gypsum	Illite, quartz, dolomite, gypsum	<63	84.60	–	–	–	–	–	–	–	–	–
			10–63	6.54	2472	0.31	13	2.49	0.47	–	–	–	–
			4–10	1.76	4393	0.31	19	2.78	0.27	0	100	33	67
			2–4	1.41	5702	0.31	20	2.82	0.26	0	100	30	70
			1–2	1.51	8271	0.31	22	2.95	0.24	0	100	52	48
			0.4–1	2.67	16439	0.32	21	2.92	0.24	0	100	59	41
			0.2–0.4	0.73	12676	0.40	18	2.77	0.25	75	25	80	20
			<0.2	0.61	9550	0.43	14	2.50	0.28	80	20	97	3

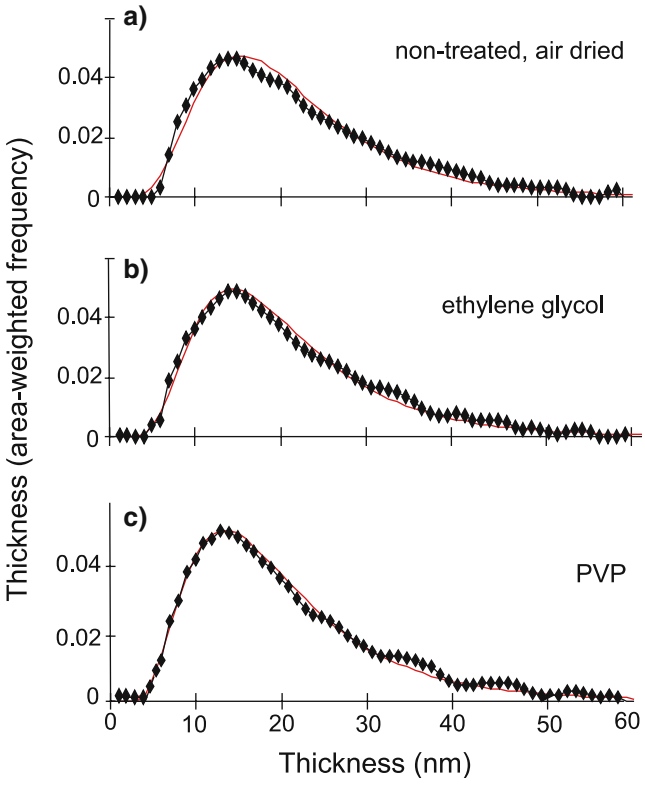

Fig. 3 *CTDs* calculated for different sample treatments of the vein at 2,176 m (0.4–1 μm). α, β^2= shape parameters defined by Eberl et al. (1986). **a** Non-treated, airdried, α=2.92, β^2=0.24. **b** ethylene glycol treated, α=2.90, β^2=0.25. **c** PVP treated, α=2.90, β^2=0.25. The various components are fitted using the Mudmaster program

by Peacor (1992) and Warr and Nieto (1998). Thin sections of ca. 100 μm thickness were prepared and small Cu-washers (1-mm diameter) adhered to the illite-rich portions of the sections. The samples were then ion-milled to the appropriate thickness and investigated using a Philips CM12 scanning-transmission electron microscope (housed at EMAL, University of Michigan), equipped with a Kevex Quantum solid-state detector. All high-resolution lattice-fringe images were resolved at a 60,000–100,000× magnification. Quantitative EDS chemical analyses were obtained in scanning TEM mode using a beam diameter of 5 nm and a scanning area of 30 × 30 nm^2. The TEM study combines lattice-fringe imaging and selected area electron diffraction (SAED) of illite polytypes, whereby compositional data were calibrated using the *k*-values of available laboratory standards (Peacor 1992). As electron diffraction analyses were not routinely undertaken during the attainment of chemical data due to analytical difficulties, variations in polytype composition could not be directly determined. An additional complication in obtaining accurate results is the partial migration and loss of mobile cations, such as K and Na, during measurements caused by beam damage (van der Pluijm et al. 1988; Peacor 1992). However, in this study this effect was not observed to be a serve problem, but may contribute to slight depletion in the interlayer cation content measured for the studied illite.

The grain-size fractions of the selected samples were analyzed by the conventional K–Ar technique (Bonhomme et al. 1975). However, the >63 μm fraction was not included to avoid contamination of biotite and K-feldspar present in some of the samples. Potassium was measured by atomic absorption with an accuracy of ±1.5%. For Ar analysis, the samples were preheated under high vacuum at 100 °C for at least 12 h to reduce the amount of atmospheric Ar^{36} adsorbed on the mineral surfaces during sample preparation and handling. The Ar isotopic compositions were compared against repeated analyses of the international GL-O standard, which averaged $24.38 \pm 0.12 \times 10^{-6}$ cm^3/g STP (2σ) of radiogenic ^{40}Ar (^{40}Ar rad) for three determinations (Table 2). The isotopic $^{40}Ar/^{36}Ar$ ratio of the atmospheric Ar was also controlled during the course of the study. As these values are close to the theoretical levels, no corrections were applied to the measured contents. As the presence of exchangeable K was considered to be minimal in this sample material, no Na exchange was undertaken.

Results

X-ray diffraction characteristics of grain-size separates

The eight separated grain-size fractions of the granite and vein samples (Table 1) are all enriched in illite with only minor amounts of other minerals. Quartz, biotite, and feldspar occur in the coarser fractions of the granite (>10 μm), whereas the finer fractions typically contain minor amounts of quartz and plagioclase. The vein assemblages contain significantly higher proportions of illite and only some traces of quartz, dolomite, or gypsum in the fine factions. Feldspars were only detected in the coarser fractions >10 μm in size (Fig. 4). The wt% of the separates reveals 5–35% of these samples to be made up of particles <10 μm in size (Table 1). In addition, based on the relative differences in peak intensity, peak area, and the XRD mineralogy, the highest abundance of illite is seen to occur in the 0.4–1 μm fractions. This trend is not so obvious in the host granite (1,570 m), due to the presence of biotite in the coarser fractions. The (001) basal

Table 2 Analytical details of the K–Ar data used

Sample (depth/m)	Grain size (μm)	K_2O (%)	^{40}Ar rad (10^{-6} cm^3/g STP)	^{40}Ar rad (%)	K–Ar age (Ma) ± 2σ
Vein-1 (1,431 m)	<2	9.46	75.5	88.0	232.4 (2.8)
	<0.2	7.44	45.9	83.6	182.0 (3.2)
Granite-1 (1,570 m)	<63	–	–	–	–
	10–63	–	–	–	–
	4–10	4.39	38.8	91.5	255.5 (6.5)
	2–4	4.34	35.3	81.6	236.4 (6.0)
	1–2	4.62	33.7	84.2	213.4 (5.2)
	0.4–1	4.77	32.8	87.2	201.4 (4.9)
	0.2–0.4	4.86	31.6	89.3	190.9 (4.6)
	<0.2	4.32	28.47	32.7	193.6 (5.7)
Granite-2 (2,167 m)	<63	–	–	–	–
	10–63	–	–	–	–
	4–10	6.74	35.4	94.0	156.1 (2.8)
	2–4	7.27	37.6	94.4	153.8 (2.5)
	1–2	8.48	38.5	94.7	135.6 (1.8)
	0.4–1	9.10	40.6	95.5	133.3 (1.7)
	0.2–0.4	8.96	32.9	91.4	110.4 (1.6)
	<0.2	8.22	25.6	85.6	93.9 (1.4)
Vein-2 (2,160 m)	<63	–	–	–	–
	10–63	–	–	–	–
	4–10	6.64	59.0	89.6	256.4 (4.6)
	2–4	7.98	65.7	94.4	238.7 (3.5)
	1–2	8.51	73.0	95.4	248.0 (3.3)
	0.4–1	9.58	78.7	99.1	238.3 (2.9)
	0.2–0.4	9.86	78.2	99.3	230.5 (2.6)
	<0.2	9.10	65.7	88.1	211.0 (2.7)
Vein-3 (2,176 m)	<63	–	–	–	–
	10–63	–	–	–	–
	4–10	9.09	88.7	97.6	279.8 (3.4)
	2–4	9.59	91.5	97.4	274.0 (3.1)
	1–2	9.81	93.7	97.4	274.3 (3.0)
	0.4–1	9.83	95.7	98.6	279.3 (3.2)
	0.2–0.4	9.73	85.0	93.2	252.3 (3.0)
	<0.2	8.54	73.2	78.0	247.9 (3.4)

reflections show large variations between the different size fractions, but they are generally broaden towards the smaller sized separates (FWHM: ~0.17–0.84°2θ).

The area-weighted CTDs calculated using the MudMaster program (Eberl et al. 1996) reveal varying best mean thickness (T) and shape (α, β^2) parameters (Table 1). Only the host granite (1,570 m) shows the typical behavior of decreasing mean thicknesses corresponding to decreasing grain size, as described in other illitic rocks (Bove et al. 2002; Dudek et al. 2002). The three other samples (one granite and two veins) show more complex trends, reflecting variable illite mixtures with the largest mean thickness occurring in the enriched 0.4–1 μm fractions. The CTDs of the grain-size fractions show two common shapes (Fig. 3): near log-normal and asymmetrical non-lognormal distributions. The complex asymmetrical distributions characterize the coarse fractions of the veins (e.g. the 4–10 μm fraction of vein-2 at 2,160 m in Fig. 5) and the altered host granite, with a notable concentration of crystallites toward smaller thicknesses. These fractions are considered to reflect prominent mixtures of different types of illite, as observed by electron microscopy, and they show the highest degree of thickness variance (β^2 values in Table 1). Volume-corrected CTDs were fitted using the program UNMIXER (provided by D. Eberl) in an attempt to group them into two populations of CTDs (a poorly crystalline distribution, pC, and a well-crystalline distribution, wC), assuming each population is characterized by a lognormal shape. The mean thicknesses were then used to calculate the % abundance of illite phases present (Table 1).

Random powder preparations confirm the physical mixture of at least two different types of illite in all samples. The occurrence of distinct reflections at 3.07 and 3.66 Å indicate the presence of a 1M polytype of the trans-vacant variety (Drits et al. 1993). The broad nature of these reflections and raised background levels observed between 20 and 35° 2θ also suggest some degree of disordering ($1M_d$ polytype). The other

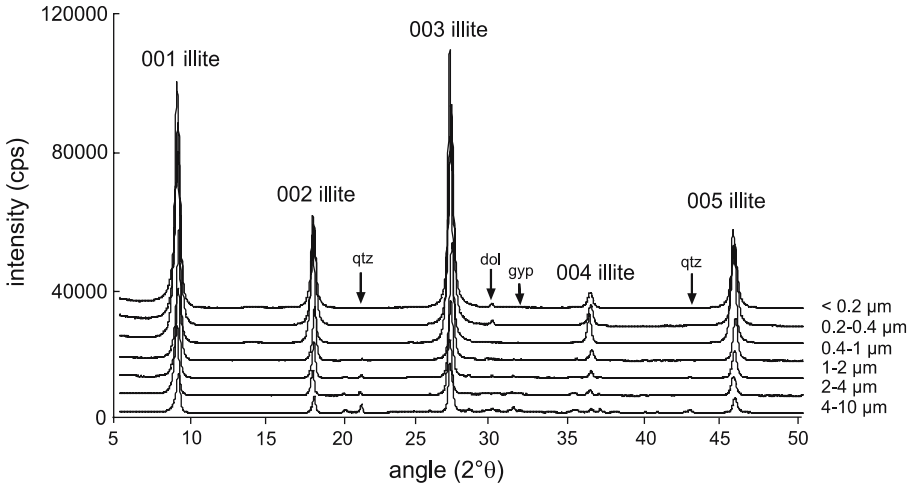

Fig. 4 Typical orientated X-ray diffraction patterns of the eight different grain sizes in the vein at 2,176-m depth. The separates of both the granite (not shown here) and the vein samples are enriched in illite with a minor amount of accessory minerals, particularly quartz in the coarse (>1 µm) fractions and dolomite in the finest (<0.4 µm) grain sizes

prominent reflections observed at 3.88, 3.49, 3.2, 2.98, and 2.86 Å characterize a $2M_1$ illite (Moore and Reynolds 1997). The intensity of these diagnostic reflections shows consistent variations with grain size (Fig. 6). The 1M polytype peaks slightly increase toward finer grain sizes, whereas the $2M_1$ reflections progressively decrease toward the finer fractions. These trends are apparent in the illite-rich vein samples, but are difficult to resolve in the polymineralic granite samples due to the overlap of feldspar reflections.

Illite microscopic characteristics

SEM images reveal a variety of illite crystal sizes and shapes in the hydrothermally altered granite and vein samples studied. Relatively large illite of a platy shape, commonly around 5–10 µm in basal length, is most abundant in the argillite veins (Fig. 7a, b). The crystals are generally pseudo-hexagonal in shape, commonly arranged in stacks, and display some sutured crystal edges suggestive of particle dissolution. A number of microstructures can be observed in the vein samples with local and poorly developed microfolds and associated hinge porosity (Fig. 7a), as well as anastomosing fabrics (Fig. 7b). TEM lattice-fringe images of the platy vein illite reveal the internal structure of the stacks. Thick packets of the $2M_1$ illite polytype can be recognized showing similar contrast and hence orientation (Fig. 7c). Their thickness ranges up to 80 nm, with high-angle grain boundaries developed between adjacent stacks. Closer examination of the packets reveals the presence of numerous high-contrast fringes and low-angle domain boundaries, producing crystallite thicknesses commonly around 10 nm. The crystallites show notable lateral variations in thickness (Fig. 7d), and are associated with zones of lattice distortion. These features imply that at least some of these crystallites represent low-angle subgrain boundaries formed by the migration of crystal defects during intracrystalline deformation (Warr and Peacor 2002).

An additional type of illite is recognized in the vein samples and adjacent granite based on crystal size and shape. Here, a network of thin and fibrous illite occurs in pore spaces (Fig. 8a). The crystals may reach over 10 µm in length, but are notably thin and commonly <1 µm broad. Crystal shapes range from fibrous needles to flat blades (Fig. 8b) and form a network of illite crystals without any observable preferred orientation, but sometimes they do occur as grain coatings. TEM lattice-fringe images and electron diffraction study of this illite reveal an array of thin 1M crystallites with notable contrast differences between individual

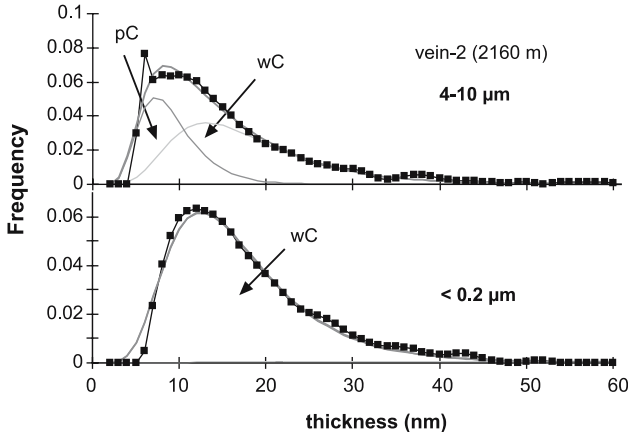

Fig. 5 Area-weighted *CTDs* of two grain-size fractions from the vein at 2,160 m, calculated using the MUDMASTER program. More complex asymmetrical distributions characterize the coarse fraction of the vein (4–10 µm), reflecting a physical mixture of two different types of illite. The smallest grain sizes (<0.2 µm) show more lognormal shapes and are considered to present the dominance of a single illite phase. *pC* poorly crystalline phase; *wC* well-crystalline phase

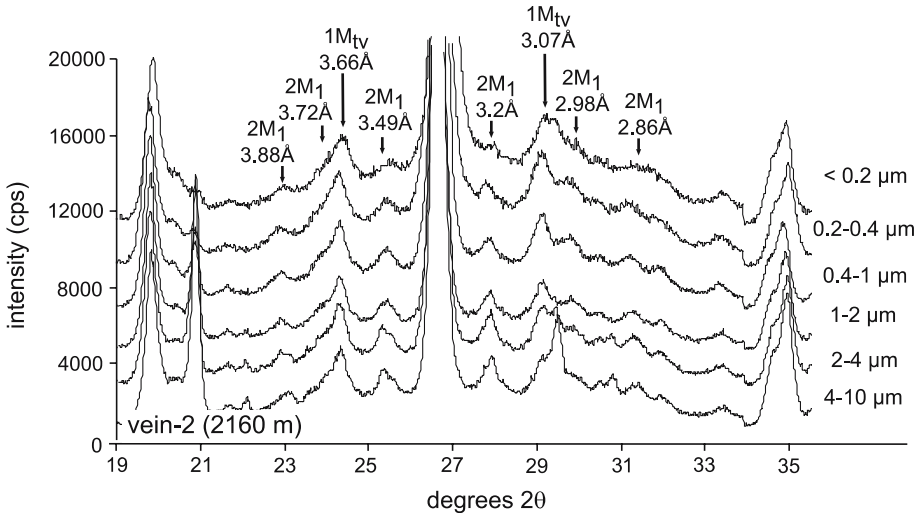

Fig. 6 Random powder preparations of the eight grain-size fractions of the vein-2 sample (2,160 m) indicate the presence of a 1M polytype of trans-vacant variety, as well as $2M_1$ illite polytype. The broad nature of the 1M reflections and raised background between 20 and 35 °2θ suggest some disordering ($1M_d$ variety). The intensity of these diagnostic reflections shows consistent variations with grain size

packets. Both discrete spots and some streaking of non-basal reflections can be observed, indicating various degrees of disorder of the 1M polytype (Fig. 8c). The crystallites are laterally continuous, contain numerous layer terminations, and are separated by distinct low-angle crystallite boundaries. In contrast to the platy vein illite, many of these crystallite boundaries probably represent crystal growth surfaces rather than sub-grain boundaries.

Illite compositions

The structural formulae of illite (normalized to $O_{10}(OH)_2$) based on AEM analyses show a broad range of compositions, but no recognizable core depth variations. The K content ranges from muscovite compositions (~1.0 per unit) to depleted interlayer values of 0.4 per $O_{10}(OH)_2$, which are usually more typical for illite–smectite minerals. As no mixed-layering was detected in these samples (Fig. 3), there are two factors capable of explaining the low K in pure illite: (1) substitution of K by Na or NH_4 or (2) very thin illite crystals with a fixed K deficiency. The latter mechanism of K-deficiency is favored here because the samples containing the smallest crystallites are generally those that are most depleted in K, and there are no analytical indications of substitution reactions occurring. The most K-enriched illite, with an average composition of $K_{0.92}(Al_{1.5}Fe_{0.17}Mg_{0.08})[Si_{3.34}Al_{0.66}]O_{10}(OH)_2$, was recorded from the altered host-rock granite-2 in the lower section of the borehole (2,167-m depth; Figs. 2, 7a). However, the most K-enriched vein illite was measured in the uppermost argillite vein-1 (1,431-m depth), with a typical composition of around $K_{0.8}(Al_{1.65}Fe_{0.21}Mg_{0.13})[Si_{3.27}Al_{0.73}]O_{10}(OH)_2$. The most K-depleted illite was recorded in vein-2 at 2,160 m, just 7 m above the sample containing the most K-rich illite within the granite.

Significant variation in composition is observed when plotting interlayer K against octahedral Fe for the vein illite, with a general trend ranging from low K and Fe to high K and Fe varieties (Fig. 9a). This trend indicates that Fe substitution in octahedral sites is related to variation in interlayer charge and thus K content. In these AEM analyses, we do not consider much Fe contamination has occurred from finely dispersed iron oxides, as such mineral phases were not observable in the areas selected for measurement.

The octahedral cation content (Al–Mg–Fe; elements listed in order of abundance) of illite also shows notable differences between host-rock granite and veins at similar depths in the borehole (Fig. 9b), but there is no consistent pattern of Fe–Al–Mg exchange. The most variable compositions are observed in the host-rock illite, with Al–Mg–Fe varieties (Fig. 9b) characterizing the pervasively altered host rock (1,570 m) and Al–Fe–Mg varieties (Fig. 9c) within fractured granite (2,167 m). In contrast, the composition of the vein illite shows less variation, with two main types of composition distinguishable. In the upper section, the vein illite has an Al–Fe–Mg octahedral content (Fig. 9b) and in the lower, brecciated vein a Mg–Fe–Al content (Fig. 9c).

K–Ar values of the different grain-size fractions

A systematic decrease in K–Ar values with decreasing grain size can be recognized for most of the granite and vein samples (Table 1). This indicates that the mixtures contain illite of different ages, with the younger phases concentrated in the finer-grain-sized fractions and the older phase dominating the coarser separates. The

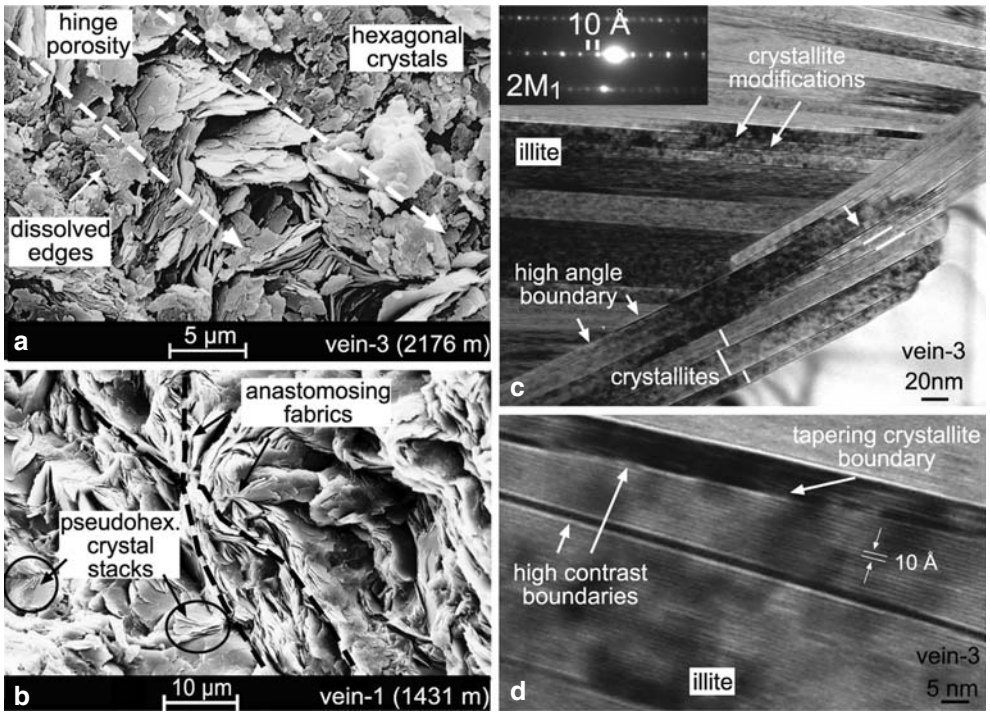

Fig. 7 Electron microscopy images of typical vein illite. **a** *SEM* image of relatively large platy illite showing pseudo-hexagonal crystal shapes and some irregular, sutured crystal edges (2,176 m). Note the occurrence of the local and poorly developed microfolds and associated hinge porosity. **b** *SEM* image of vein illite showing the local development of an anastomosing fabric with pseudohexagonal crystal stacks (1,431 m). **c**, **d** *TEM* lattice-fringe images of illite stacks showing subparallel thick packets containing numerous thinner crystallites (ca. 10–15-nm thickness) attributed to intracrystalline deformation. The *SAED* images (*top left*) show the $2M_1$ nature of the illite polytype (2,176 m)

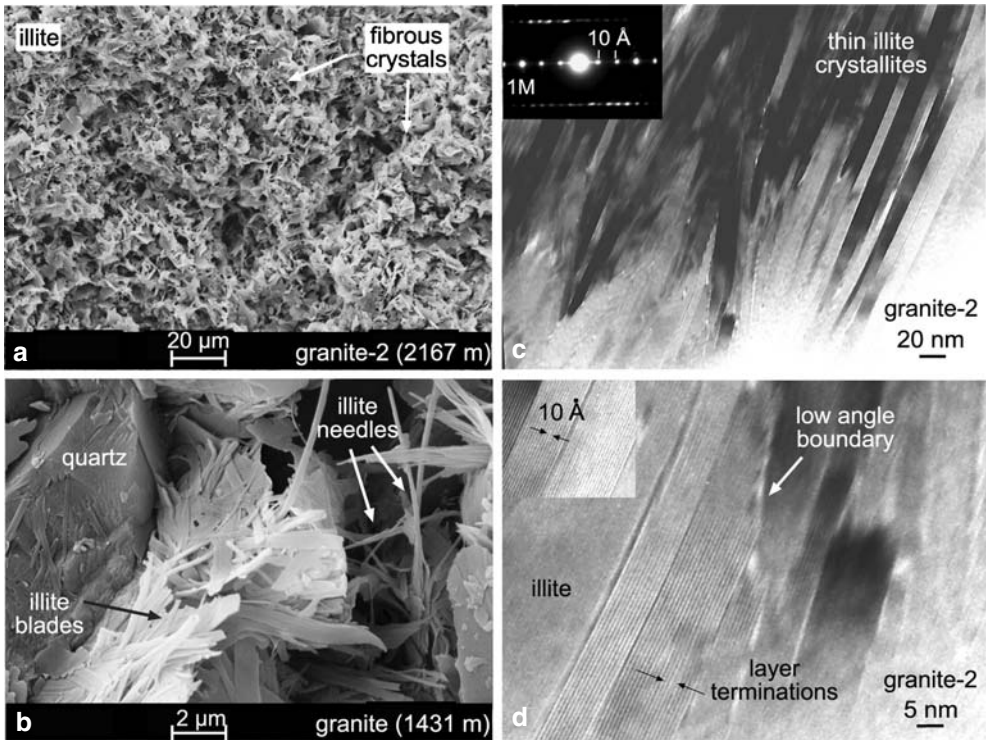

Fig. 8 Electron microscopy images of typical granite-host rock illite (2,167 and 1,431 m). **a** Network of thin, flaky, or fibrous illite have grown in the pore spaces, where the crystals are notably thin. **b** Crystal shapes range from fibrous needles to flat blades with no visual preferred orientation, but sometimes they do occur as grain coatings. **c** *TEM* lattice-fringe images show high-contrast and tapering crystallite boundaries. The crystallites are more laterally continuous, contain numerous layer terminations, and are separated by distinct low-angle crystallite boundaries. *SAED* patterns (*top left* in **c**) show typical 1M polytypes (2,167 m)

K–Ar values of the separated grain sizes of the five samples studied (two granites and three veins) are plotted together in Fig. 10. The oldest K–Ar values are recorded in the vein-3 sample from the deeper section of the borehole (2,176 m). Here, two groups of age values can be recognized, the oldest around 274–280 Ma in the >1 μm fractions, and the youngest around 247–252 Ma in the <1 μm sizes. In contrast, the other samples show a more continuous and progressive decrease in age values with decreasing grain size. The

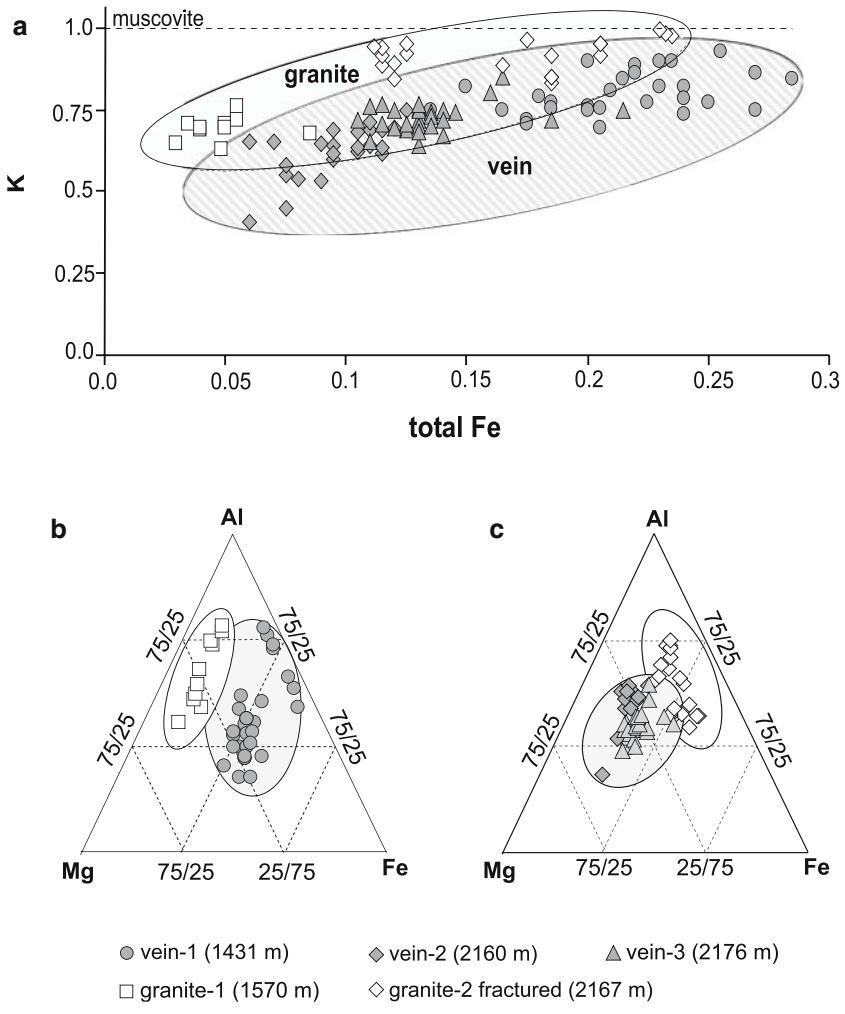

Fig. 9 Composition of illite in the altered host granite samples and the argillaceous mineral veins. **a** Plot of interlayer K versus total Fe showing the wide range of K and Fe contents. **b** Triangular Al–Mg–Fe plots showing compositional variations related to octahedral occupancy

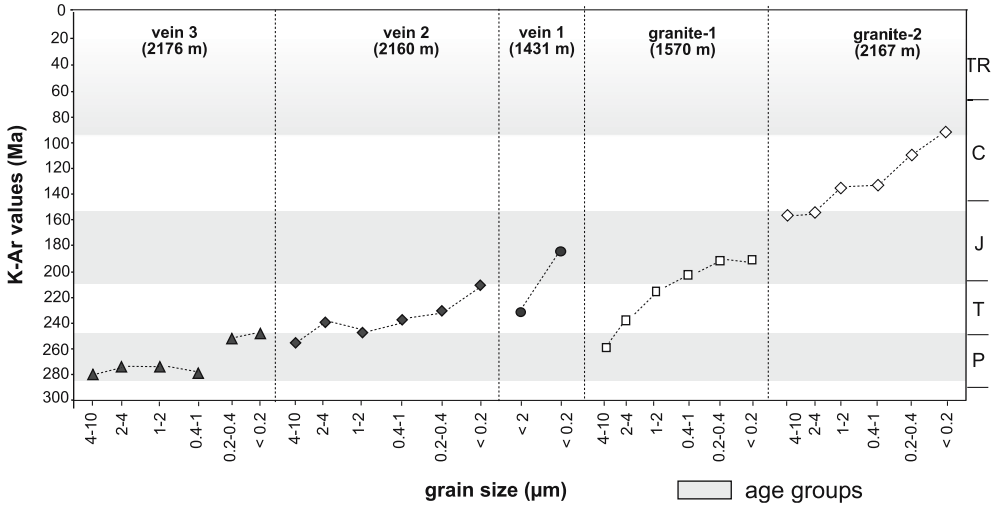

Fig. 10 K–Ar values of the separated grain-size fractions of two granite samples and three vein samples showing the principal stages of illite crystallization. Based on the distributions of these K–Ar values with varying grain size, three age groups can be recognized. The oldest group (ca. 247–280 Ma) corresponds to a Permian age and are dominant in the veins. A second group corresponds to Jurassic ages (ca. 153–194 Ma) and is present in both veins and granite. The youngest age group is present in the finest fraction of the granite-2 sample, and is Cretaceous (< ca. 94 Ma) or younger in range

oldest value of vein-2 at 2,160 m in the coarsest fraction (4–10 μm) is ca. 256 Ma, which corresponds well with the youngest group of values outlined for vein-3. The lowest value of this vein-2 is ca. 211 Ma, which is recorded from the <0.2 μm fraction. Only two grain sizes (<0.2 and <2 μm) were determined in the vein-1 sample from the upper part of the borehole (1,431-m depth). They provide a value at ca. 182 Ma for the fine fraction and ca. 232 Ma for the coarse fraction.

The ca. 256 Ma end-member value of veins 2 and 3 is also present in the coarse 4–10 μm fraction of the pervasively altered granite-1 sample at 1,570 m. The lowest values of this sample are younger than the sequence of vein-2, forming a plateau at about 190–194 Ma in the fractions <0.4 μm. A significantly younger range of K–Ar values characterizes the fractured host-rock granite at 2,167 m. The oldest values of the coarser fraction (4–10 μm) again show a narrow plateau at ca. 153–156 Ma, whereas the youngest end-member occurs in the finest (<0.2 μm) fraction at ca. 94 Ma.

On the basis of the described distribution of K–Ar values with varying grain sizes, three main age groups can be recognized from the sample suite (gray bands in Fig. 10). The oldest K–Ar age group (ca. 247–280 Ma) corresponds to Permian ages, which are preserved in vein-3 and in the coarsest fraction of vein-2 and granite-1. A second K–Ar age group of Jurassic age (ca. 153–194 Ma) is best defined in the finest fraction of granite-1 and the coarsest fraction of granite-2. The youngest age group recognized in this study is of Cretaceous age or younger (<94 Ma), here recorded only in the <0.2 μm fraction of granite-2.

Analysis of illite mixtures based on K–Ar values, polytypes, and CTDs

To decipher the contributions of the individual illite populations from the described mixtures and to evaluate the end-member age values of the involved components, the K–Ar results are plotted against both the abundance of the $2M_1$ polytype and the % mean crystallite thicknesses (volume-weighted) of the fitted well-crystalline CTDs (Fig. 11). Plotting the % $2M_1$ polytype content against K–Ar values of vein-3 (Fig. 11a) confirms well the values previously estimated on the basis of the variations of K–Ar results relative to the different grain sizes (Fig. 10). Two equivalent apparent plateaus can be recognized in vein-3, suggesting that two separate phases of Permian

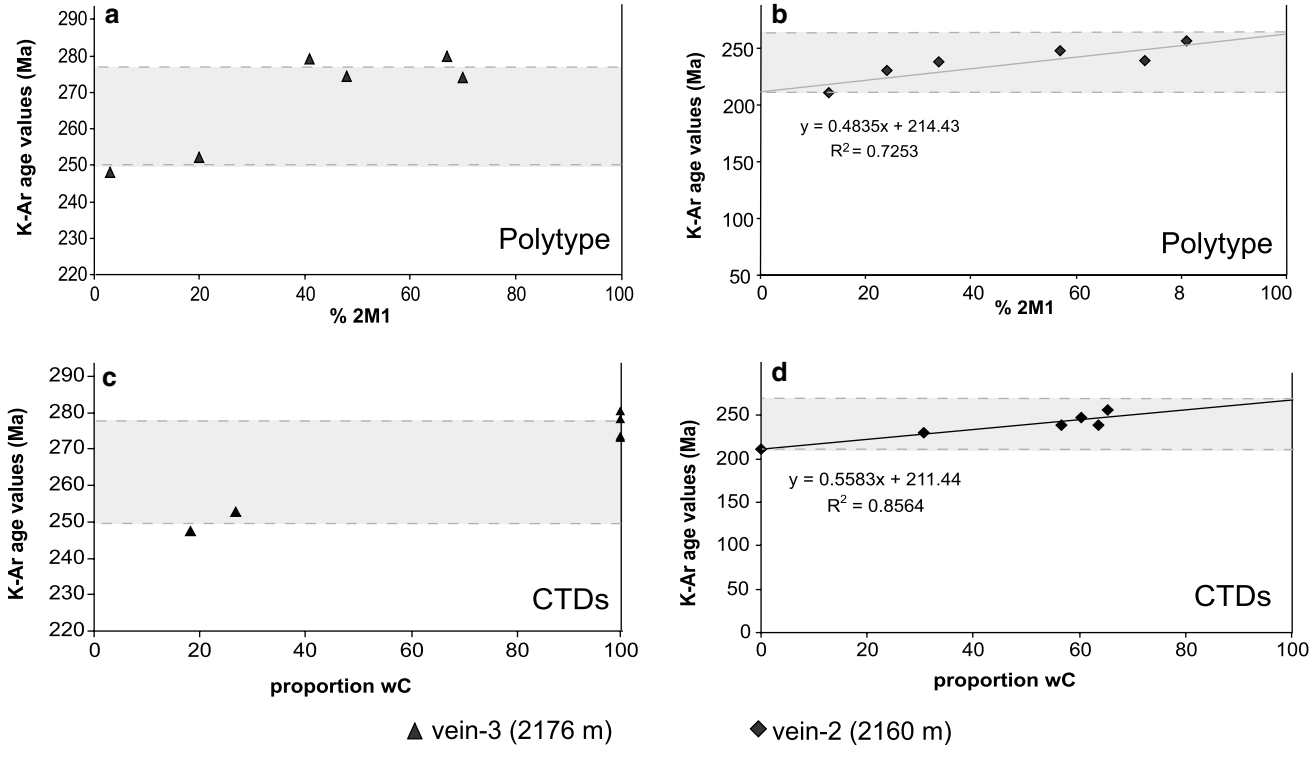

Fig. 11 K–Ar values plotted against the abundance of the $2M_1$ polytype (**a**, **b**) and volume-weighted % mean crystallite thickness of the well-crystalline (*wC*) size distribution (**c**, **d**) for vein-3 and vein-2. The intercepts on the *y*-axis at 0% $2M_1$ and 0% *wC* represent the age of the 1M illite polytypes, and the *y*-axis intercept at 100% $2M_1$ and 100% *wC* are the ages of the $2M_1$ crystals

crystallization occurred. However, each plateau consists of a mixture of both types of polytype crystals, indicating that structural transformations may have formed during single crystallization events. Two equivalent plateaus of Permian age are also observed when plotting the K–Ar age values against the % thicknesses of wC distribution (Fig. 11c), but the estimated mixtures are not equal to those determined by polytype content. According to the UNMIXER program, all coarse fractions >1 μm in size contain just one population of illite crystallites, despite containing different polytypes.

The vein-2 sample shows a mixture of polytypes and CTDs for the different measured grain sizes (Fig. 11a, c). Fitting a linear regression to the polytype mixtures give a reasonable correlation coefficient (R^2=0.73), with intercepts of axes representing either the 1M or the $2M_1$ end-member. They indicate ages in accordance to those estimated from the K–Ar grain-size data of the sample suite, with a pure $1M_{tv}$ end-member age value of ca. 215 Ma and a pure $2M_1$ age value of ca. 260 Ma. The vein-2 sample also yields intercepts at ca. 210 and 270 Ma for the pC and wC end-members, respectively (Fig. 11d).

Discussion

The timing and mechanism of episodic illite crystallization

The main argillaceous product of the hydrothermally altered Soultz-sous-Forêts granite studied here is illite, which is generally <10 μm in size and comprises ca. 3–11% of the total rock weight (Table 1). On the basis of our combined XRD, SEM, TEM, and isotopic results, a number of episodic illite crystallization events can be recognized in each of the granite and vein samples. In general, they are characterized by differences in crystal size, shape, microstructure, polytype, composition, and K–Ar age values. Useful information concerning the timing and mechanism of these episodic events can be deduced from the eight grain-size separates prepared for each sample, with mixtures of two main types of illite crystals: well-crystalline platy $2M_1$ and poorly crystalline fibrous 1M trans-vacant varieties showing various degrees of disorder (Figs. 5, 6). The pattern of K–Ar values for the two granites and the three veins reveals different mixtures of Permian, Jurassic, and Cretaceous (or younger) age groups (Fig. 10).

Permian illite is largely of the $2M_1$ polytype and occurs in the coarse fractions of all samples, except granite-2. This polytype is known to form in epithermal conditions at temperatures ranging between 125–350 °C (Velde 1965). Despite similar appearance, a range of illite compositions occurs in samples dominated by the $2M_1$ polytype, with significant variations in both the K and octahedral cation contents (Fig. 9), indicating a link between them. However, there is no clear indication that these variations relate to the temperature of illite formation. For example, K-depleted platy illite occurs in one of the deeper vein samples at 2,160 m. The observed compositional variations are thus considered more likely to reflect variations in fluid compositions and in the fluid–rock ratio experienced by the various parts of the granite body (Durst and Vuataz 2000; Pauwels et al. 1993). The characteristic Mg–Al-rich and Fe-poor octahedral contents, with low-to-moderate amounts of interlayer K (0.4–0.75 per unit formula) of the vein and the granite samples, are dominated by finer illite and probably reflect the composition of post-Variscan Permian fluids.

The deepest vein sample (2,176 m) of similar composition contains thick, platy $2M_1$ illite crystals of Permian age that are split up into numerous sub-grains, forming 10-nm thick domains (Fig. 7c). The high-contrast fringes mark the sites of planar defects and do not represent low-charged smectitic layers. The formation of subgrains during intracrystalline deformation reduces the mean crystallite thickness, and splits the $2M_1$ crystals into a number of smaller X-ray scattering domains. Sub-grain formation implies relatively enhanced temperature conditions accompanied by intracrystalline strain, presumably associated with the formation of the vein rock fabric (Warr and Peacor 2002). The mineralization of Permian illite marks the formation and thus the age of vein opening related to the circulation of late-Variscan to post-Variscan, hydrothermal CO_2-rich fluids of higher temperatures (180–340 °C) and moderate salinity (2–7 wt% eq. NaCl), which are preserved as inclusions in quartz veins at similar depths within the borehole (Dubois et al. 1996).

This lower vein sample (2,176 m) actually shows two plateaus or age populations of apparent Early and Late Permian ages (Fig. 10). Each population contains a mixture of $2M_1$ and 1M polytypes of the same isotopic age, which may represent evolving stages of crystallization occurring in response to the inflow of episodic Permian hydrothermal fluids. In such a scenario, the progressive cooling history of each fluid pulse, or changes in the saturation state of the fluid, could explain the transition from 2M to 1M polytypes observed in each population. Another possible explanation for the Late Permian cluster in this sample is the presence

of younger, post-Permian illite occurring only in the < 0.4 μm fraction. However, extrapolation of the end-member ages from the pure 1M phases based on the K–Ar versus polytype plot gives an intercept modeled age of ca. 245 Ma, implying no younger illite in this sample (Fig. 10).

Jurassic or Cretaceous (or younger) aged illite is present in most samples as either $2M_1$ or 1M polytypes. The latter polytype occurs as fine-grained, elongated fibrous to lath-shaped crystals (< 1 μm broad) of the trans-vacant variety (Figs. 6, 8). Such trans-vacant 1M polytypes are typical for pure hydrothermal illite and have been described in a number of case studies (Grathoff and Moore 2002; Rosenberg 2002). This polytype is generally considered to form under lower temperature conditions than $2M_1$ varieties, and probably formed during migration of younger brines of around 130–170 °C, associated with the main alteration of biotite and plagioclase in the granite (Aquilina et al. 1997; Dubois et al. 1996). The younger 1M fibrous illite varieties also grew partly at the expense of older, platy illite. It is therefore possible that some inherited argon may have been incorporated into newly crystallized phases. Younger illite of Cenozoic Tertiary age (N. Liewig, pers. comm.) has been reported in the finest grain-sized fractions extracted from fracture coatings of the Soultz-sous-Forêts granite.

The composition of the 1M illite can only be estimated from granite samples abundant in these phases. Here, fine-grained fractions yield a similarly broad range of K and Fe/Mg variations, as described for the platy $2M_1$ crystals, but the K-content of the fibrous varieties in the fractured granite host rock is notably high (Fig. 9). Similar types of diagenetic fibrous illite are well documented in the Permian Mesozoic sediments of North Sea basins and northern Germany (Zwingmann et al. 1998; Wilkinson and Haszeldine 2002), and are considered to form under low-temperature diagenetic conditions. The pore-filling fibrous varieties of illite are clearly younger and are probably related to partial dissolution of the older $2M_1$ platy phases, as well as plagioclase crystals.

Although the Permian age of illite appears to be relatively well established, the true age of the Mesozoic (or younger) illite is more difficult to define accurately on the basis of K–Ar ages alone. In considering both the polytype and CTD results, and the timing of illite crystallization, it becomes apparent that the transition from 2M to 1M polytypes has occurred at least three or four times over a period of ca. 200 Ma. Each transition may be viewed as a hydrothermal event representing the progressive cooling of fluids. This can also be applicable to the Permian events, where the different polytypes have similar K–Ar age values. However, this mechanism of formation alone is unlikely to apply to the polytype transitions that show large age differences between end-member K–Ar values. It is considered more probable that the rock permeability was a key factor controlling the polytype transition, which in turn influenced the saturation state of the pore fluids. It is evident that the 1M trans-vacant variety characterized by lognormal CTDs grew largely as fibrous illite in the restricted pore space of both the granite matrix and the veins. These features are compatible with crystal growth within a closed or restricted system (Eberl et al. 1998a, b). Reduced rock-permeability conditions (Surma and Geraud 2003) were favorable for concentrating supersaturated pore fluids and the rapid growth of lath or fibrous crystals (Mullin 1961), similar to those documented in sandstones of the North Sea (Wilkinson and Haszeldine 2002). A strong permeability and fluid saturation control on the illite crystallization would also explain the large range of illite compositions recorded in the alterations of the Soultz-sous-Forêts granite.

Conclusions

1. At least three episodes of hydrothermal illite crystallization occurred in the fractured granite and veins of the Soultz-sous-Forêts granite. Based on assessment of grain-size-dependent K–Ar values, and the modeled end-member ages determined from K–Ar versus polytype plots, illitization events are suggested to have occurred during Permian, Jurassic, and Cretaceous (or younger) times. K–Ar age determinations based on crystal thickness distributions confirmed these results.
2. Each granite and vein sample studied contains two main types of illite: a higher temperature pseudo-hexagonal $2M_1$ polytype and a lower temperature 1M trans-vacant variety. The latter polytype occurs largely as lath and fibrous-shaped crystals.
3. The K–Ar analyses indicate that all samples contain different mixtures of illite ages. The differences observed in the distribution of illite ages, polytypes, crystallite thicknesses, and compositions suggest that the timing and mechanism of argillite crystallization varied in different parts of the granite. The primary influence on the nature of illite crystallization appears to have been the temperature and composition of percolating hydrothermal fluids. However, here the rock permeability was also a key determining factor, with the transition from platy 2M to more fibrous 1M

polytype structures corresponding to the progressive sealing of both fractured granite matrix and mineralized veins.

4. The argillite veins are suggested to have formed during a Permian hydrothermal event related to CO_2-rich fluids. Additional sealing events also occurred during Mesozoic and younger times, which correspond to the percolation of lower-temperature saline brines.

Acknowledgments This study was funded by the GRK 273 ''Fluid–rock-interaction'' grant of the DFG, Germany. We thank Ben van der Pluijm and Don Peacor (Michigan) for supporting the TEM work. Special thanks also to Jana Just and Agnes Kontny for numerous helpful discussions. Dennis Eberl is thanked for providing the UNMIXER program. Raymond Wendling and Thierry Perrone (CGS Strasbourg) are thanked for technical assistance during the K–Ar determinations (this is EOST publication # 2006.302).

References

Alexandrov P, Royer JJ, Deloule E (2001) 331 ± 9 Ma emplacement age of the Soultz monzogranite (Rhine Graben basement) by U/Pb ion-probe zircon dating of samples from 5 km depth. Earth Planet Sci 332:747–754

Altaner SP, Ylagan RF, Savin SM, Aronson JL, Belkin HE, Pozzuoli A (2003) Geothermometry, geochronology, and mass transfer associated with hydrothermal alteration of a rhyolitic hyaloclastite from Ponza Island, Italy. Geochim Cosmochim Acta 67(2):275–288

Aquilina L, Pauwels H, Genter A, Fouillac C (1997) Water–rock interaction processes in the Triassic sandstone and the granitic basement of the Rhine Graben: geochemical investigation of a geothermal reservoir. Geochim Cosmochim Acta 61:4281–4295

Bailey SW, Hurley PM, Fairbairn HW, Pinson WH Jr (1962) K–Ar dating of sedimentary illite polytypes. Geol Soc Am Bull 73:1167–1170

Bonhomme M, Thuizat R, Pinault Y, Clauer M, Wendling R, Winkler R (1975) Methode de datation potassium-argon. Appareillage techniques. Note Technique de l'Institute de Géologie de Strasbourg 3, p53

Bove DJ, Eberl DD, McCarty DK, Meeker GP (2002) Characterization and modeling of illite crystal particles and growth mechanisms in a zoned hydrothermal deposit, Lake City, Colorado. Am Mineral 87:1546–1556

Clauer N, Chaudhuri S (1995) Clays in crustal environments: isotope dating and tracing. Springer, Berlin Heidelberg New York

Clauer N, Kröner A (1979) Strontium and argon isotopic homogenization of pelitic sediment during low-grade regional metamorphism: the Pan-African upper Damara sequence of northern Namibia. Earth Planet Sci Lett 43:117–131

Clauer N, Naoual R, Schaltegger U, Piqué A (1995a) K–Ar systematics of clay-to-mica minerals in a multi-stage low-grade metamorphic evolution. Chem Geol 124:305–316

Clauer N, O'Neil JR, Furlan S (1995b) Clay minerals as records of temperature conditions and duration of thermal anomalies in the Paris Basin, France. Clay Miner 30:1–13

Clauer N, Liewig N, Pierret M, Toulkeridis T (2003) Crystallization conditions of fundamental particles from mixed-layer illite–smectite of bentonites based on isotopic data (K–Ar, Rb–Sr and delta (super ^{18}O)). Clays Clay Miner 51:664–674

Drits V, Weber F, Salyn AL, Tsipursky SI (1993) X-ray identification of one layer illite varieties: application to the study of illite around uranium deposits of Canada. Clays Clay Miner 41:389–398

Drits V, Srodon J, Eberl DD (1997) XRD measurement of mean crystallite thickness of illite and illite/smectite: reappraisal of the Kübler index and the Scherrer equation. Clays Clay Miner 45:461–475

Dubois M, Ayt Ougoudal M, Meere P, Royer J, Boiron M, Cathelineau M (1996) Temperature of paleo- to modern self-sealing within a continental rift basin: the fluid inclusion data (Soultz-sous-Forêts, Rhine Graben, France). Eur J Mineral 8:1065–1080

Dudek T, Srodon J, Eberl DD, Elsass F, Uhlik P (2002) Thickness distribution of illite crystals in shales. I. X-ray diffraction vs. high-resolution transmission electron microscopy measurements. Clays Clay Miner 50:562–577

Durst P, Vuataz FD (2000) Fluid–rock interactions in hot dry rock reservoirs: a review of the HDR sites and detailed investigations of the Soultz-sous-Forêts system. In: Proceedings of the world geothermal congress 2000, Kyushu-Tohoku, 28 May–10 June 2000

Eberl DD, Srodon J, Mingchou L, Nadeau PH, Northrop H (1987) Sericite from the Silverton Caldera, Colorado: correlation among structure, composition, origin, and particle thickness. Am Mineral 72:914–934

Eberl DD, Drits VA, Srodon J, Nueesch R (1996) MUDMASTER: a program for calculating crystallite size distributions and strain from the shapes of X-ray diffraction peaks. Open-File Report. U.S. Geological Survey, Report: of 96-0171 ftp://www.brrcrftp.cr.usgs.gov/pub/ddeberl/

Eberl DD, Drits VQ, Srodon J (1998a) Deducing growth mechanisms for minerals from the shapes of crystal size distributions. Am J Sci 298:499–533

Eberl DD, Nueesch R, Sucha V, Tsipursky S (1998b) Measurement of fundamental illite particle thicknesses by X-ray diffraction using PVP-10 intercalation. Clays Clay Miner 46:89–97

Elsass P, Aquilina L, Beauce A, Benderitter Y, Fabriol H, Genter G, Pauwels H (1995) Deep structures of the Soultz-sous-Forêts HDR site. In: Proceedings of the world geothermal congress, Florence, pp 2543–2647

Genter A, Traineau H (1991) Geological survey of the HDR borehole EPS-1, Soultz-sous-Forêts, Alsace-France. BRGM, R32433

Genter A, Traineau H (1996) Analysis of macroscopic features in granite in the HDR geothermal well EPS-1, Soultz-sous-Forets, France. J Volcanol Geotherm Res 72:121–141

Genter A, Traineau H, Ledesert B, Bourgine B, Gentier S (2000) Over 10 years of geological investigations within the HDR Soultz project, France. In: Proceedings of the world geothermal congress 2000, Kyushu-Tohoku, 28 May–10 June 2000

Glasmacher UA, Tschernoster R, Clauer N, Spaeth G (2001) K–Ar dating of magmatic sericite crystallites for determination of cooling paths of metamorphic overprints. Chem Geol 175:673–687

Grathoff GH, Moore D (2002) Characterization of the Waukesha illite: a mixed-polytype illite in the Clay Mineral Society repository. Am Mineral 87:1557–1563

Grathoff GH, Moore DM, Hay RL, Wemmer K (2001) Origin of illite in the lower Paleozoic of the Illinois Basin: evidence for brine migration. Geol Soc Am Bull 113:1092–1104

Honty M, Uhlik P, Sucha V, Caplovicova M, Francu J, Clauer N, Biron A (2004) Smectite to illite alteration in salt-bearing bentonites: the East Slovak Basin. Clays Clay Miner 52:533–551

Hower J, Hurley PM, Pinson WH, Fairbairn HW (1963) The dependence of K–Ar age on the mineralogy of various particle size ranges in a shale. Geochim Cosmochim Acta 27:405–410

Hunziker JC, Frey M, Clauer N, Dallmeyer RD, Friedrichsen H, Flehming W, Hochstrasser K, Roggwiller P, Schwander H (1986) The evolution of illite to muscovite: mineralogical and isotopic data from the Glarus Alps, Switzerland. Contrib Mineral Petrol 92:157–180

Imaoka T, Nakashima K, Itaya T, Okada T (2001) Timing and duration of hydrothermal activity in the Oligocene Hamada Cauldron, SW Japan: evidence from K–Ar ages of sericite. Resour Geol (Tokyo 1998) 51:55–62

Inoue A, Meunier A, Beaufort D (2004) Illite–smectite mixed-layer minerals in felsic volcaniclastic rocks from drill cores, Kakkonda, Japan. Clays Clay Miner 52:66–84

Kim J, Peacor DR (2002) Crystal-size-distribution of clays during episodic diagenesis: the Salton Sea geothermal system. Clays Clay Miner 50:371–380

Laverret E. (2002) Evolutions temporelles et spatiales des alterations argileuses des gisements d'uranium sous discordance, secteur de Shea Creek (bassin de l'Athabasca, Canada). Unpublished thesis de l'Université de Poitiers

Ledesert B, Berger G, Meunier A, Genter A, Bouchet A (1999) Diagenetic-type reactions related to hydrothermal alteration in the Soultz-sous-Forêts Granite, France. Eur J Mineral 11(4):731–741

Liewig N, Clauer N (2000) K–Ar dating of varied microtextural illite in Permian gas reservoirs, northern Germany. Clay Miner 35:271–281

Merriman RJ, Frey D (1999) Patterns of very low-grade metamorphism in metapelitic rocks. In: Frey M, Robinson D (eds) Low-grade metamorphism. Blackwell, p 313

Montigny R, Faure G (1969) Contribution au probleme de l'homogeneisation isotopique du strontium des roches totales au cours du metamorhisme. Cas du Wisconsin Range, Antarctique. Comptes Rendus à l'Académie des Sciences, Paris 268D:1012–1015

Moore DM, Reynolds RC (1997) X-ray diffraction and the identification and analysis of clay minerals. Oxford University Press, pp 378

Mullin JW (1961) Crystallization. Butterworths, UK

Pauwels H, Fouillac C, Fouillac AM (1993) Chemistry and isotopes of deep geothermal saline fluids in the Upper Rhine Graben: origin of compounds and water rock interactions. Geochim Cosmochim Acta 57:2737–2749

Peacor DR (1992) Diagenesis and low-grade metamorphism of shales and slates. In: Buseck PR (ed) Minerals and reactions at atomic scale: transmission electron microscopy. Rev Mineral 27:335–380

Pribnow D, Clauser C (2000) Heat and fluid flow at the Soultz hot dry rock system in the Rhine Graben. In: Proceedings of the world geothermal congress, Kyushu-Tohoku, 28 May–10 June 2000

Reuter A (1985) Grain-size dependency of K–Ar dating and illite crystallinity determined on anchizonal metapelites and associated metatuffs from the eastern Rhenish Schiefergebirge. Goettinger Arbeiten zur Geologie und Palaeontologie 27:91

Rosenberg PE (2002) The nature, formation and stability of end-member illite: a hypothesis. Am Mineral 87:103–107

Rousset D, Clauer N (2003) Discrete clay diagenesis in a very low-permeable sequence constrained by an isotopic (K–Ar and Rb–Sr) study. Contrib Mineral Petrol 145:182–198

Sausse J, Genter A, Leroy JL, Lespinasse M (1998) Description and quantification of vein alterations: paleopermeabilities in the Soultz-sous-Forêts granite (Bas-Rhin, France). Bull Soc Geol Fr 169:655–664

Schleicher (2005) Clay mineral formation and fluid–rock interaction in fractured crystalline rocks of the Rhine rift system: case studies from the Soultz-sous-Forêts granite (France) and the Schauenburg Fault (Germany). Doctorate Thesis, University of Heidelberg, pp 104

Srodon J (1984) X-ray identification of illitic materials. Clays Clay Miner 32:337–349

Srodon J, Clauer N, Eberl DD (2002) Interpretation of K–Ar dates of illitic clays from sedimentary rocks aided by modeling. Am Mineral 87:1528–1535

Surma F, Geraud Y (2003) Porosity and thermal conductivity of the Soultz-sous-Forêts granite. Pure Appl Geophys 160:1125–1136

van der Pluijm BA (1999) Clay-bearing fault gouge: processes and implications. Goettinger Arbeiten zur Geologie und Palaeontologie Sonderband 4:158

van der Pluijm BA, Lee JH, Peacor DR (1988) Analytical electron microscopy and the problem of potassium diffusion. Clays Clay Miner 36(19):498–504

van der Pluijm BA, Hall CM, Vrolijk PJ, Pevear DR, Covey MC (2001) The dating of shallow faults in the Earth's crust. Nature 412:172–174

Velde B (1965) Experimental determination of muscovite polymorph stabilities. Am Mineral 50:436–449

Warr LN, Nieto F (1998) Crystallite thickness and defect density of phyllosilicates in low-temperature metamorphic pelites: a TEM and XRD study of clay–mineral crystallinity-index standards. Can Mineral 36:1453–1474

Warr LN, Peacor DR (2002) Evaluation of X-ray diffraction methods for determining the crystal growth mechanisms of clay minerals in mudstones, shales and slates. Schweizerische Mineralogische Petrografische Mitteillungen 82:187–202

Wilkinson M, Haszeldine RS (2002) Fibrous illite in oilfield sandstones—a nucleation kinetic theory of growth. Terra Nova 14:56–60

Yates DM, Rosenberg PE (1998) Characterization of neoformed illite from hydrothermal experiments at 250 °C and $P_{v,soln}$: an HRTEM/ATEM study. Am Mineral 83:1199–1208

Ylagan RF, Kim CS, Pevear DR, Vrolijk PJ (2002) Illite polytype quantification for accurate K–Ar age determination. Am Mineral 87:1536–1545

Zwingmann H, Clauer N, Gaupp R (1998) Timing of fluid flow in a sandstone reservoir of the North-German Rotliegend (Permian) by K–Ar dating of related hydrothermal illite. In: Parnell J (ed) Dating and duration of fluid flow events. Geol Soc Lond Spec Publ 144:91–106